Journal of Materials Chemistry C

PAPER

View Article Online
View Journal | View Issue

Cite this: J. Mater. Chem. C, 2016, 4, 4546

Influence of alkyl side-chain length on the carrier mobility in organic semiconductors: herringbone *vs.* pi–pi stacking†

Zhiying Ma,[a] Hua Geng,*[b] Dong Wang*[a] and Zhigang Shuai[ab]

Received 22nd February 2016,
Accepted 2nd April 2016

DOI: 10.1039/c6tc00755d

www.rsc.org/MaterialsC

The influence of the alkyl side-chains on the electronic structures, molecular packing and charge transport for five naphthalene diimide (NDI) derivatives, four [1]benzoselenopheno[3,2-*b*][1]benzoselenophene (BSBS) derivatives and three [1]benzothieno[3,2-*b*]benzothiophene (BTBT) derivatives is systematically investigated by density functional theory calculations coupled with a tunneling enabled hopping model. The results show that the introduction of long alkyl chains does not affect the energy levels of frontier molecular orbitals and reorganization energies, but can modify the molecular packing in organic semiconductors. It is found that for the π–π stacking systems such as NDI derivatives and **BSBS-C10/C14**, the charge mobility decreases with alkyl chain length, which is due to the displaced stacking along the short axis of the molecular plane, while for the herringbone stacking systems such as BTBT derivatives and **BSBS-C8/C12**, the charge mobility increases with alkyl chain length, due to enhanced π···π interaction along the stacking direction and the displaced stacking along the short axis of the molecular plane, respectively.

1. Introduction

Organic semiconductors have received great attention for application in field-effect transistors,[1,2] light-emitting diodes,[3–5] and photovoltaics.[6–8] Particularly, solution processing is one of the most attractive features of organic semiconductors due to the advantages such as low cost and large-area device fabrication.[9] In order to design ideal air-stable organic transport materials, much effort has been devoted to modifying the conjugated backbones.[10–13] Side chains attached to the conjugated cores, such as alkyl, oligo(ethylene glycol), and fluoroalkyl, are usually introduced to ensure solubility for device fabrication. Generally speaking, side chains are considered as insulating materials, and do not directly contribute to charge transport in organic devices. However, there has been increasing attention to side chain engineering due to the substantial impact of side chains on charge mobility, by affecting either the inter-molecular packing or the thin film morphology in the solid state.[14–16]

Alkyl chains are the most commonly employed side chains in conjugated molecules.[11] In fact, from the studies based on the same conjugated backbones, it can be found that even a subtle change of the alkyl chains may result in substantial influence on charge transport properties.[16] Chain lengths,[17–21] branching positions,[17,18,22–26] odd–even effects,[27,28] and chirality[29] of alkyl chains can all affect the charge carrier mobility.[16] Firstly, the alkyl chains with an appropriate length have been shown to increase the charge mobility significantly for a number of conjugated small molecule[17] and polymer semiconductors.[18–21] The increase of the charge carrier mobility has been accounted for by the improved surface morphology for copolymers containing dithiophene units and dithienyl-diketopyrrolopyrrole (DPP) with branched alkyl chains of 2-octyldodecyl (2-C8C12) or 2-decyltetradecyl (2-C10C14).[18] It was also attributed to the shortened π–π distances in polymers containing (*E*)-2-(2-(thiophen-2-yl)vinyl)thiophene units and dithienyl-(DPP) with branched alkyl chains of 2-C8C12 or 2-C10C14.[19] Improved crystalline ordering for polymers containing thienothiophene and dithienyl-(DPP) units carrying branched alkyl chains of 2-hexyldecyl (2-C6C10) or 2-C8C12 has also been argued.[20] Nevertheless, by increasing the alkyl chain length from 2-C6C10 to 2-C8C12, the decrease of the charge carrier mobility of the devices formed by the thiophene–diketopyrrolopyrrole based quinoidal small molecules was caused by the poor crystalline ordering.[17] Secondly, it was found that the branching position of the alkyl chains has noticeable influence on the charge transport for both small molecule[17,25,26] and polymer[18,22–24] semiconductors. Previous studies showed that gradually moving the branching position away from the backbone could gradually decrease π–π stacking distances and lead to an increase of the charge carrier mobility.[17,18,22–24] The devices based on thiophene–diketopyrrolopyrrole with an alkyl

[a] *MOE Key Laboratory of Organic Optoelectronics and Molecular Engineering, Department of Chemistry, Tsinghua University, 100084 Beijing, P. R. China*
[b] *CAS Key Laboratory of Organic Solids, Institute of Chemistry, Chinese Academy of Sciences, 100190 Beijing, P. R. China. E-mail: hgeng@iccas.ac.cn*
† Electronic supplementary information (ESI) available. See DOI: 10.1039/c6tc00755d

chain branched at the third carbon position displayed the most best performance.[17] For the DPP polymers, the best performance devices were obtained by using the branched alkyl chains of 4-decylcetyl (4-C10C16)[18] and 5-decylheptadecyl (5-C10C17),[22] respectively. The devices exhibiting high mobilities were formed by benzodifurandione-based poly(*p*-phenylene vinylene) and the isoindigo-based conjugated polymers with branched alkyl chains of 4-octadecyldocosyl (4-C18C22)[23] and 4-decyltetradecyl (4-C10C14),[24] respectively. However, the movement of the branching alkyl chain position away from the backbone does not always improve the film quality.[17,23] Thirdly, the odd–even effect of alkyl chains exerts its influence on crystal packing and charge transport. Akkerman *et al.*[27] reported the odd–even effect of the alkyl-substituted diphenylbithiophene (P2TP) systems. The results showed that despite the pronounced odd–even effect in the tilt angle with increasing alkyl chain length for the film structure, no clear odd–even effect of dependence of alkyl chain length on mobility was observed in FET measurements, which is likely due to the contribution of several layers to the charge transport and other limiting factors for the charge transport. Back *et al.*[28] investigated a series of diketopyrrolopyrrole-selenophene vinylene selenophene (DPP-SVS) polymers, ranging from 25-DPP-SVS to 32-DPP-SVS with branched alkyl groups containing linear spacer groups from C2 to C9. Spacer groups with even numbers of carbon atoms exhibited shorter lattice spacing than did spacer groups with odd numbers of carbon atoms, resulting in one order of magnitude higher charge mobility. Finally, to investigate the stereoisomerism effect of alkyl chains, Liu *et al.* separated and identified three stereoisomers of DPP(TBFu)$_2$, *i.e.*, the mesomer, *RR*-isomers and *SS*-isomers.[29] The *RR*- and *SS*-isomers have similar crystal structures, thin-film morphologies, and FET properties. The mesomer has the best FET performance due to its shorter π–π stacking, which is about 4 times higher than that of the *RR*- and *SS*-isomers.

Alkyl side-chains attached to the conjugated backbone may introduce two competing effects: the steric hindrance and the intermolecular dispersive attraction. Firstly, the steric hindrance of the alkyl chains with the backbone could be minimized by moving the branching point away from the backbone; thus small molecules or polymers present gradually decreasing π–π stacking distances, resulting in increasing mobility.[22,24] Nevertheless, a closer π–π stacking distance does not always correlate with higher mobility.[23] Secondly, the chain–chain interactions ascribed to attractive dispersion forces systematically increase with increasing alkyl chain length and are the main source of the increase in the total cohesive energy;[30] thus polymers present decreased π–π stacking distances, resulting in increasing mobility.[19] As a result, choosing an appropriate alkyl chain as a substituent is becoming an important strategy to design high performance organic semiconductors. To date, there have been very few theoretical studies on the influence of the alkyl chain length on the charge transport properties of small-molecule organic semiconductors, which have shown that the transfer integrals with longer alkyl chains ($n \geq 5$) have isotropic values and those with shorter alkyl chains become highly anisotropic.[30]

In this work, we are interested in the influence of alkyl chain length on the charge mobility of small-molecule organic semiconductors. Naphthalene diimides are a class of extensively investigated electron transport organic semiconductors.[11] In general, these materials exhibit good conducting properties. Their geometries and electronic properties can be obtained through variation of the substituents on the imide nitrogen atoms or in the naphthalene core. It was found that naphthalene diimides with alkyl chain substituents on the imide nitrogen atoms exhibited different magnitudes of electron mobility.[31,32] On the other hand, [1]benzothieno[3,2-*b*]benzothiophene (BTBT) derivatives[11,33–37] and [1]benzoselenopheno[3,2-*b*][1]benzoselenophene (BSBS) derivatives[11,33,38] have been widely employed as hole transport materials in organic field-effect transistors. When the alkyl chains have been introduced into the BTBT molecule, *i.e.* BTBT-C8, BTBT-C10, and BTBT-C12, the order of the overall field-effect mobility is BTBT-C12 > BTBT-C10 > BTBT-C8 in BTBT-based devices.[36] However, the charge carrier mobility of BTBT-C8 can reach as high as 31.3 cm^2 V^{-1} s^{-1} based on its single crystal films.[34] The theoretical study by a mixed molecular dynamics and quantum-chemical methodology showed that the effect of dynamic disorder on charge transport can be neglected.[39] The dihedral angle dependence of transfer integrals in BTBT exhibited a pattern much different from the conventional organic semiconductors and showed that a considerable magnitude of transfer integral was expected in the large dihedral angle region.[40] For the BSBS derivatives, the introduction of alkyl chains of different lengths can induce charge carrier mobility of different magnitudes.[38] These phenomena are consistent with what we all know, the performance of organic semiconductor based devices depends on the length of alkyl chains attached to their main backbone. Therefore, we systematically study the charge transport properties of NDI, BSBS, and BTBT molecules with different lengths of alkyl chains.

2. Theoretical and computational methodology

Since the charge transfer process often coupled intramolecular high frequency vibration in organic semiconductors, we employed the tunneling enabled hopping model to describe the charge transport, which has been shown to give a reasonable description.[41–43] In this model, each hopping event is viewed as a non-adiabatic electron transfer reaction, *i.e.*, the charge transfer (for electron) between two adjacent molecules follows the reaction M + M$^-$ → M$^-$ + M, where M is the molecule undergoing the electron transfer. The quantum mechanical charge transfer rate, under the perturbation theory and the displaced harmonic oscillator approximation, can be deduced from the Fermi Golden Rule

$$k_{if} = \frac{1}{\hbar}|V_{fi}|^2 \int_{-\infty}^{\infty} dt \times \exp\left\{ i\omega_{fi}t - \sum_j S_j\left[(2\bar{n}_j + 1) - \bar{n}_j e^{-i\omega_j t} - (\bar{n}_j + 1)e^{i\omega_j t}\right]\right\} \quad (1)$$

Here, V_{fi} is the transfer integral between the final and initial states. For the self-exchange reaction, $\omega_{fi} = \Delta G^{\circ}/\hbar$ goes to zero, where ΔG° is the Gibbs free energy difference between the final state and the initial state. $S_j = \lambda_j/\hbar\omega_j$ is the Huang–Rhys factor of the j-th normal mode, which is a measure of the electron–phonon coupling strength. ω_j and λ_j are the vibrational frequency and reorganization energy of the vibrational mode j, respectively. $\bar{n}_j = 1/(e^{\hbar\omega_j/k_BT} - 1)$ is the phonon occupation number of the j-th normal mode. It should be noted that the convergence of the numerical integration of eqn (1) can be achieved by choosing the vibrational mode with the largest Huang–Rhys factor with short time approximation.

From eqn (1), it can be seen that the electron transfer integral V_{fi}, vibrational frequency ω_j, and the Huang–Rhys factor S_j are three important parameters to determine the charge transfer rate. The transfer integrals for the nearest-neighbor dimers along the transport pathways in bulk crystals are calculated using the site energy correction method,[44–46] which reads

$$V_{mn} = \frac{V^0_{mn} - \frac{1}{2}(e_m + e_n)S_{mn}}{1 - S_{mn}^2} \quad (2)$$

Here, $V^0_{mn} = \langle \Phi_m|H|\Phi_n\rangle$, $e_{m(n)} = \langle \Phi_{m(n)}|H|\Phi_{m(n)}\rangle$ and $S_{mn} = \langle \Phi_m|S|\Phi_n\rangle$, where $\Phi_{m(n)}$ is the lowest unoccupied molecular orbital (for electron transport) or the highest occupied molecular orbital (for hole transport) of the isolated molecule m or n in the dimer. H and S are the dimer Hamiltonian and the overlap matrices, respectively. The positive values of the transfer integrals indicate the bonding interaction between the isolated molecules in the dimer (frontier orbital coupled with the same phase), and negative values of the transfer integrals indicate an antibonding interaction (frontier orbital coupled with the inversed phase) of the corresponding frontier orbital. The sign of transfer integrals only indicates the combination type of the frontier orbital. All the calculations of transfer integrals are performed using density functional theory with the PW91PW91 functional in combination with the 6-31G* basis set. This approach has been found to give reasonable results.[39,47] The vibrational frequencies of the normal modes for the neutral and anion states (or cation states) associated with the electron (hole) transfer process are calculated using the Gaussian 09 program[48] with the B3LYP functional and the 6-31G* basis set. The Huang–Rhys factor S_j and the reorganization energy λ_j of every normal mode can be calculated using the DUSHIN program.[49] Generally speaking, reorganization energy has both internal λ_{int} and external λ_{ext} contributions. The former reflects the geometric relaxation of individual molecules upon going from the neutral to the charged state and *vice versa*. And the latter reflects the electronic polarization of the surrounding molecules, which is usually neglected.[50] The internal reorganization energy is dominant and can be evaluated either from the adiabatic potential-energy surfaces[51] or from the normal-mode analysis.[49] The latter approach can provide the partition of the internal reorganization energy into the contributions from each vibrational mode:

$$\lambda_{int} = \sum \lambda_i = \sum \hbar\omega_i S_i = \sum \frac{1}{2}\omega_i^2 \Delta Q_i^2 \quad (3)$$

Here, ΔQ_i represents the displacement along the normal mode i between the equilibrium geometries of the neutral and charged molecules.

Within the hopping model, the charge mobility can be expressed by the Einstein relation:

$$\mu = \frac{e}{k_B T} D \quad (4)$$

The diffusion coefficient D is calculated by the kinetic Monte Carlo simulation approach. We take one molecule arbitrarily as the initial charge center. The charge is only allowed to hop to the nearest neighbor molecules. The hopping probability is evaluated as $p_\alpha = k_{mn} \Big/ \sum_{n'} k_{mn'}$, where k_{mn} is the hopping rate from site m to n, and n' represents all nearest molecules. The residence time of the carrier at site m is $1 \Big/ \sum_{n'} k_{mn'}$. At each step, a random number is uniformly generated between 0 and 1. If $\sum_{\alpha=1}^{n-1} p_\alpha < r \leq \sum_{\alpha=1}^{n} p_\alpha$, the hopping distance is taken to be the intermolecular centroid distance. The charge then goes to the neighbor in the α-th direction as the nearest position of the charge. By repeating the simulation process, thousands of simulations should be performed to get a linear relationship between the mean-square displacement and the simulation time to get the diffusion coefficient. Finally, the mobility can be obtained from the Einstein relation.

In addition, to better understand the nature of noncovalent interaction between alkyl chains, the total interaction energies and magnitudes of the noncovalent interaction between two molecules are calculated by symmetry-adapted perturbation theory (SAPT),[52] which is a basis set superposition error free energy partition method. SAPT provides decomposition of the interaction energy into physically meaningful components, *i.e.*, the electrostatic, dispersion, induction and exchange. In SAPT, the Hamiltonian of a dimer is partitioned into contributions from each monomer and the interaction as

$$H = F_A + W_A + F_B + W_B + V \quad (5)$$

Here, the Hamiltonian is written as a sum of the usual monomer Fock operator F, the Møller–Plesset fluctuation operator of the monomers W, and the perturbation operator of the interaction between the two monomers V. F is treated as the zeroth-order Hamiltonian and the interaction energy is evaluated through a perturbative expansion of V and W. The first-order correction represents the classical electrostatic interaction and its corresponding exchange correction. The second-order polarization correction is divided into induction and dispersion components. The simplest truncation of SAPT is denoted as SAPT(0) which computes terms to the second order with respect to inter-monomer electron correlation and neglects intramonomer electron correlation. The energy can be written as

$$E_{SAPT(0)} = E^{(10)}_{elst} + E^{(10)}_{exch} + E^{(20)}_{ind,resp} + E^{(20)}_{exch\text{-}ind,resp} + E^{(20)}_{disp} + E^{(20)}_{exch\text{-}disp} \quad (6)$$

In this notation, $E^{(vw)}$ defines the order in V and W; the subscript resp indicates that orbital relaxation effects are included. The Psi4 code[53] is employed for these calculations, with the SAPT(0)[54,55] used in conjunction with the truncated version of the aug-cc-pVDZ (*i.e.* jun-cc-pVDZ) basis set. The two-electron integrals for SAPT(0) are computed with the density fitting (DF) approximation.

3. Results and discussion

3.1 Electronic structure

All the compounds investigated here are illustrated in Fig. 1. The crystal structures are taken from the Cambridge Structure Database. All the molecular geometries have been optimized at the B3LYP/6-31G(d) level of theory starting from the crystal structure. The energy levels and distributions of the frontier molecular orbitals of the compounds have been obtained at the same level of theory. As presented in Fig. 2, taking the compounds with the shortest and longest alkyl chains as examples, respectively, we find that both HOMO and LUMO are spread over the whole rigid π-conjugated skeletons. Especially, for the naphthalene diimide, the substitution position of the alkyl chains locates at the nodes and there is no density distribution on the substitution groups. On the other hand, for the BTBT derivatives and BSBS derivatives, the alkyl chain substituents make only very little contribution to the HOMO and LUMO. Thus, alkyl chains with different lengths cannot affect the energy level of frontier molecular orbitals of the systems. This can be seen from the values of HOMO and LUMO orbitals as presented in Table 1.

Adiabatic electron affinity (AEA) is the energy difference between a neutral species and its anionic species. And adiabatic ionization potential (AIP) is the energy difference between cationic and neutral species. From previous studies, the adiabatic electron affinities of air-stable n-channel materials are in the range of 2.41 eV to 3.14 eV and the adiabatic ionization potentials of air-stable p-channel materials are in the range of 5.905 eV to 7.02 eV.[56] The adiabatic electron affinities (AEA) and ionization potentials (AIP) of the alkyl chain derivatives are shown in Table 1. AEA values of NDI derivatives fit well for the air-stable n-channel materials. Moreover, the AIP values of BTBT derivatives and BSBS derivatives are within the range of AIP values for air-stable p-channel materials. The alkyl chain length has little effect on the values of AEA and AIP.

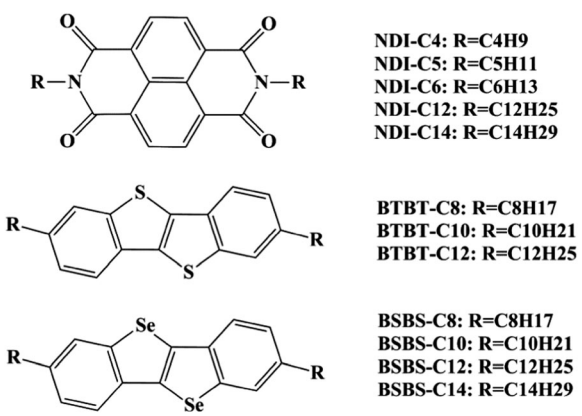

Fig. 1 Chemical structures of NDI, BTBT, and BSBS derivatives.

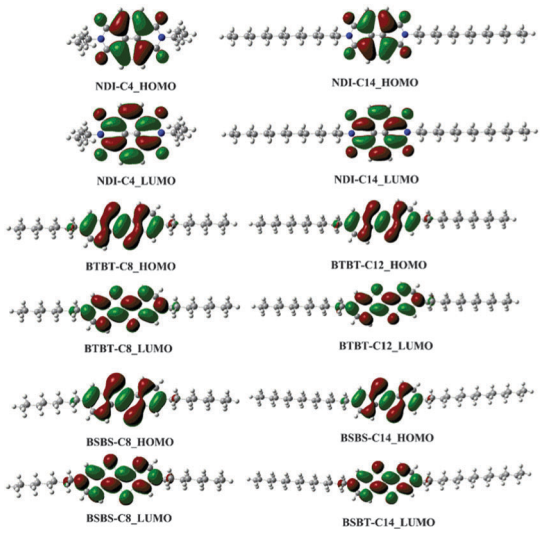

Fig. 2 Distributions of the HOMOs and LUMOs of NDI, BTBT, and BSBS derivatives.

Table 1 The calculated LUMOs, HOMOs, adiabatic electron affinities (AEA), adiabatic ionization potentials (AIP), and inner-sphere reorganization energies (RE)

Complexes	LUMO[a] (eV)	HOMO[a] (eV)	AEA[a] (eV)	AIP[a] (eV)	RE (meV)
NDI-C4	−3.72	−7.28	2.46		351
NDI-C5	−3.70	−7.27	2.46		350
NDI-C6	−3.70	−7.27	2.46		351
NDI-C12	−3.70	−7.27	2.46		350
NDI-C14	−3.70	−7.27	2.46		350
BTBT-C8	−1.40	−5.60		6.84	246
BTBT-C10	−1.39	−5.60		6.84	246
BTBT-C12	−1.39	−5.60		6.84	252
BSBS-C8	−1.45	−5.54		6.78	227
BSBS-C10	−1.45	−5.54		6.78	226
BSBS-C12	−1.44	−5.54		6.78	226
BSBS-C14	−1.44	−5.54		6.78	227

[a] The values are obtained from single point energy calculations at the B3LYP/6-31+G(d) level of theory based on the optimized geometries at the B3LYP/6-31G(d) level of theory.

3.2 Reorganization energy

The reorganization energy is an essential molecular parameter. The calculated values of all compounds are shown in Table 1. NDI derivatives are very close to each other, and the same can be found for BTBT and BSBS derivatives. That is to say, the reorganization energies barely change with the increasing length of alkyl chains, as the alkyl chain makes few contributions to the frontier orbitals of the whole molecules.

The reorganization energy can be decomposed into all the vibration mode relaxations, as shown in Fig. 3 for **NDI-C14**, **BTBT-C12**, and **BSBS-C14**. For **NDI-C14**, the distribution profiles

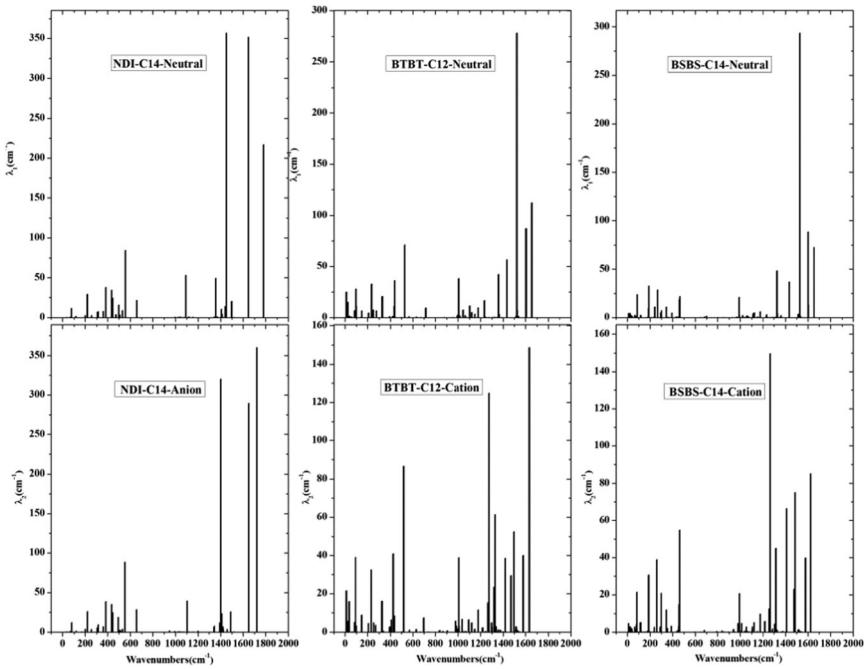

Fig. 3 The contributions of the vibrational modes to the geometry relaxation for neutral and charged states of **NDI-C14**, **BTBT-C12**, and **BSBS-C14**.

in both neutral states and anion states are similar, with one bunch of modes in the low frequency region (around 500 cm^{-1}) and the other in the high frequency region (around 1500 cm^{-1}). The contribution from the high frequency region, which mainly arises from the C=C in-plane stretching motion in the conjugated core, is much larger than that from the low frequency modes. A similar distribution of the mode-decomposed contribution to the reorganization energy can be seen in **BTBT-C12** and **BSBS-C14**. Previous studies showed that the high-frequency vibration should be treated fully quantum mechanically.[43] Therefore, the nuclear quantum effect needs to be taken into account when calculating the charge transfer rate.

3.3 Transfer integral

The charge transport properties of organic semiconductors are highly sensitive to the relative orientations and packing characters of the organic molecules. According to the crystal structure of the systems and the calculated transfer integrals, we divide the studied systems into two categories: π–π stacking and herringbone stacking, as shown in Fig. 4 and 7. For comparison,

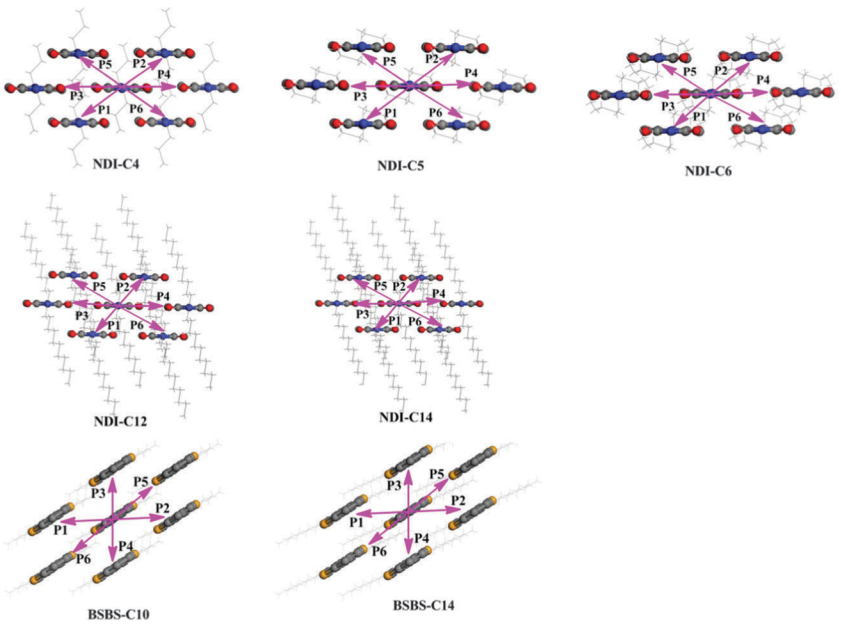

Fig. 4 Schematic illustration of charge hopping pathways for NDI derivatives and BSBS derivatives (π–π stacking).

Table 2 The transfer integrals V (in meV) and centroid distance d_C (in Å) along major hopping pathways selected based on the crystal structures of NDI derivatives and BSBS derivatives

		P1	P2	P3	P4	P5	P6
NDI-C4	d_C	5.223	5.223	9.123	9.123	7.840	7.840
	V	130	130	17	17	41	41
NDI-C5	d_C	5.028	5.028	9.540	9.540	8.107	8.107
	V	93	93	11	11	38	38
NDI-C6	d_C	4.888	4.888	9.334	9.334	8.265	8.265
	V	69	69	14	14	28	28
NDI-C12	d_C	4.610	4.610	8.944	8.944	6.590	6.590
	V	−31	−31	20	20	25	25
NDI-C14	d_C	4.637	4.637	8.989	8.989	6.637	6.637
	V	−31	−31	20	20	22	22
BSBS-C10	d_C	5.614	5.614	7.296	7.296	9.205	9.205
	V	89	89	16	16	−2	−2
BSBS-C14	d_C	5.565	5.565	7.332	7.332	9.204	9.204
	V	78	78	16	16	−2	−2

the π-conjugated backbone with no alkyl chain substituents (*i.e.* **NDI-C0**, **BTBT-C0**, **BSBS-C0**) has also been considered. Obviously, **NDI-C0** also adopts the π–π stacking and **BTBT-C0** and **BSBS-C0** adopt the herringbone stacking, while the structures of these π-conjugated backbones with no alkyl chain are changed markedly compared with those of systems with alkyl chains. Thus the main concern of this paper is to focus on the properties of the latter. More details of the properties of π-conjugated backbones with no alkyl chains are provided in the ESI.†

3.3.1 π–π stacking. As presented in Fig. 4, five NDI derivatives and two BSBS derivatives adopt the π–π stacking layered configuration. The lateral displacements of the stacking pairs along the short-axis and the long-axis as well as the vertical distances depend on the length of alkyl side-chains. It is noted that the transfer integrals along **P1** and **P2** pathways are much larger than for the other pathways, as presented in Fig. 4 and Table 2.

On the other hand, as listed in Table 2 the transfer integrals along a similar pathway exhibit large variations with the length of alkyl chains for either NDI or BSBS derivatives, although the crystal stacking configuration is similar as illustrated in Fig. 4. In order to investigate the influence of the alkyl chain length on the molecular packing, we only consider the dimers possessing the maximal transfer integral (**P1** and **P2**) for NDI derivatives and BSBS derivatives. The calculated transfer integrals and the corresponding intermolecular distances, including the centroid distances of the selected dimers, the perpendicular distance between the NDI or BSBS core planes, and the displacements along the molecular short and long axis as defined in Fig. 5, are provided in Table 3. Obviously, the absolute values of transfer integrals of the NDI derivatives decrease with the increasing length of alkyl chains. The same behavior has also been found for the BSBS derivatives. We first look at the NDI derivatives. The transfer integrals are determined directly by three independent structural parameters, *i.e.*, interplane distances (d_P) and the displacements along the long (d_L) and the short (d_S) molecular axis. The centroid distances are determined by these three parameters. As we already know, the transfer integral reduces monotonically with the increase of the interplane distance between the dimers.[57,58] However, we see that with an

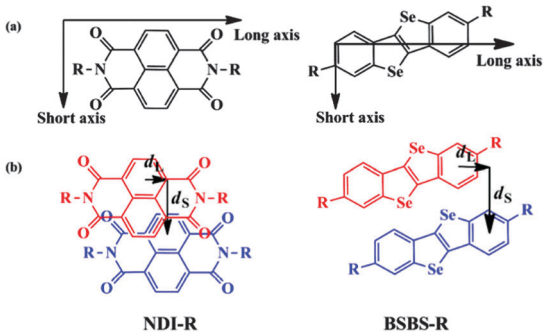

Fig. 5 (a) The definition of the long molecular axis and the short molecular axis. (b) Transverse offsets in NDI-R and BSBS-R defining two orthogonal slip directions.

Table 3 The electronic transfer integrals (in meV) and inter-molecular distances (in Å) along **P1** based on the crystal structures of NDI and BSBS derivatives

	d_C[a]	d_P[b]	d_S[c]	d_L[d]	V[e]
NDI-C4	5.223	3.323	3.805	1.408	130
NDI-C5	5.028	3.273	3.729	0.831	93
NDI-C6	4.888	3.349	3.366	1.164	69
NDI-C12	4.610	3.314	2.788	1.570	−31
NDI-C14	4.637	3.354	2.826	1.539	−31
BSBS-C10	5.614	3.030	4.386	1.666	89
BSBS-C14	5.565	3.077	4.182	1.646	78

[a] d_C refers to the distances between centroids of the dimer. [b] d_P refers to the perpendicular distances between the dimers. The least-squares plane formed by the atoms of rigid π-conjugated skeletons is needed when measuring the perpendicular distances. [c] d_S refers to the displacement along the short axis of compounds. [d] d_L refers to the displacement along the long axis of compounds. [e] V refers to the value of transfer integrals along the packing direction.

increase of the alkyl chain length, the variation of the interplane distance is so small that its influence on the transfer integrals can be neglected. Therefore, the reduction of the transfer integral from **NDI-C4** to **NDI-C14** is ascribed to the variation of displacements along the short and long axis. Similarly, for BSBS derivatives, only the displacement along the short axis from **BSBS-C10** to **BSBS-C14** reduces significantly. Thus, the reduction of transfer integrals with the increasing length of alkyl chains can be attributed to the variation of displacement along the short molecular axis.

To show how the intermolecular packing influences the transfer integral, a simple model of NDI and BSBS (R═H as illustrated in Fig. 1) is employed to discuss the evolution of the transfer integrals as a function of long molecular axis (d_L) and short molecular axis displacements (d_S) by sliding one molecule over the other in a cofacial configuration. This evolution method has also been applied to similar systems.[40,59–62] As seen above, the substituents at the imide position make no contribution to the HOMO and LUMO of all NDI compounds, and the alkyl chain substituents for BSBS derivatives make a minor contribution to the HOMO and LUMO. Therefore, we can employ the simplified models to investigate the relationship between intermolecular packing and transfer integrals. Fig. 6 gives a more

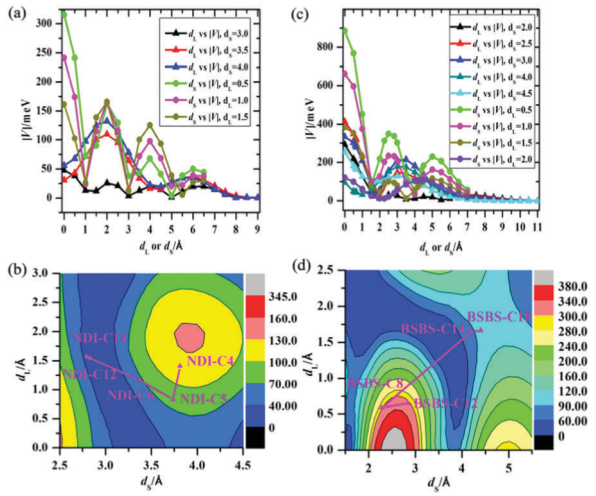

Fig. 6 Evolution of transfer integrals in absolute values (meV) with short (d_S) and long (d_L) axis displacements (as defined in Fig. 5) by sliding one molecule over the other in the NDI (a and b) and BSBS (c and d) simplified model. (a) The interplane distances are set at 3.323 Å, which is the interplane distance of the dimer along **P1** of **NDI-C4** in the crystal. The two-dimensional contour plot is (b). (c) The interplane distances are set at 3.03 Å, which is the interplane distance of the dimer along **P1** of **BSBS-C10** in the crystal. The two-dimensional contour plot is (d).

intuitive description of the sensitivity of the transfer integral to intermolecular orientation for NDI (Fig. 6a and b) and BSBS (Fig. 6c and d). According to Fig. 6a, the absolute values of electron transfer integrals are oscillating with increasing displacements along both the long molecular axis and the short molecular axis and the oscillations are more obvious when along the short axis, which are consistent with the previous study.[58,63] Moreover, the location of **P1** dimers of NDI derivatives listed in Table 3 is labelled in the two-dimensional contour plot (shown in Fig. 6b). Obviously, the relative magnitudes of electron transfer integrals of these simple models are consistent with those of dimers with alkyl chains. As illustrated in Fig. 6c, the oscillating values of the hole transfer integral along the short and long axis depend on the HOMO feature of BSBS, and the relative magnitudes of the hole transfer integral of **BSBS-C10** and **BSBS-C14** can be found in the two-dimensional contour plot (shown in Fig. 6d).

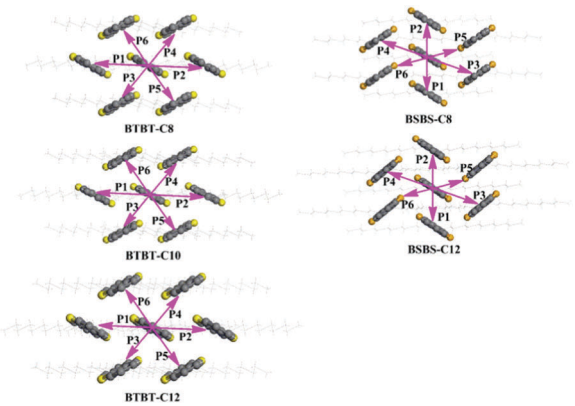

Fig. 7 Schematic illustration of charge hopping pathways for three BTBT derivatives and two BSBS derivatives.

Table 4 Dimer interaction energies (in kcal mol^{-1}) determined at the SAPT(0)/jun-cc-pVDZ level of theory, and SAPT(0) energy decompositions for the model dimers

	$E_{SAPT(0)}$	E_{elst}	E_{ind}	E_{disp}	E_{exch}
sNDI_C4	−15.67	−8.62	−2.38	−20.79	16.12
sNDI_C5	−16.19	−8.04	−2.32	−21.72	15.89
sNDI_C6	−18.78	−9.00	−2.66	−24.04	16.92
sNDI_C12	−21.50	−9.29	−2.61	−30.58	20.97
sNDI_C14	−22.10	−8.85	−2.52	−30.72	19.99

To further understand how alkyl chains affect the intermolecular interactions and the packing in NDI derivatives, the total interaction energies and magnitudes of the noncovalent interaction between two molecules are determined by SAPT. Using the crystal packing configuration, the dimers with the largest transfer integral (**P1** pathway, as presented in Fig. 4) are extracted. In order to reduce the calculation time, we consider simplified models of the molecules (named as **sNDI-C*n***, n = 4,

Table 5 The transfer integrals (in meV) and intermolecular distances (in Å) along major hopping pathways selected based on the crystal structures of BTBT derivatives and BSBS derivatives

		P1	P2	P3	P4	P5	P6
BTBT-C8	d_C[a]	5.927	5.927	4.930	4.930	4.930	4.930
	d_P[b]	2.793		(56.4)			
	d_S[c]	5.284					
	d_L[d]	0.626					
	V[e]	38	38	−7	−7	−7	−7
BTBT-C10	d_C	5.923	5.923	4.912	4.912	4.912	4.912
	d_P	2.750		(55.5)			
	d_S	5.285					
	d_L	0.656					
	V	45	45	−22	−21	−22	−21
BTBT-C12	d_C	5.864	5.864	4.855	4.855	4.855	4.855
	d_P	2.705		(55.2)			
	d_S	5.244					
	d_L	0.689					
	V	56	56	−32	−37	−37	−32
BSBS-C8	d_C	4.187	4.187	5.974	5.974	5.974	5.974
	d_P	3.525		(66.5)			
	d_S	2.275					
	d_L	0.590					
	V	−75	−75	41	41	41	41
BSBS-C12	d_C	4.401	4.401	5.782	5.782	5.782	5.782
	d_P	3.562		(74.3)			
	d_S	2.826					
	d_L	0.654					
	V	−108	−108	52	52	52	52

[a] d_C refers to the distances between centroids of the dimer. [b] d_P refers to the perpendicular distances between the dimers. The data in parentheses refer to the angle between the dimers. The least-squares plane formed by the atoms of rigid π-conjugated skeletons is needed when measuring the perpendicular distances and angles. [c] d_S refers to the displacement along the short axis of compounds. [d] d_L refers to the displacement along the long axis of compounds. [e] V refers to the value of transfer integrals along the packing direction.

5, 6, 12, 14), *i.e.*, the alkyl chain on one side of the backbone is replaced by a hydrogen atom. The packing of **sNDI-C*n*** dimers is consistent with that along **P1**. The SAPT(0) total energies and energy decompositions are presented in Table 4. Comparisons of the four components of the total energies show that the attractive dispersion energy should play a predominant role in stabilizing the dimer. The dispersion energy alone is able to provide net stabilization in each dimer as the exchange energy is smaller than the dispersion energy in absolute values. On the other hand, from the SAPT(0) interaction energies, we find that the dimers are increasingly stabilized with increasing alkyl chain length. Only the dispersion energies of **sNDI-C*n*** dimers increase with the alkyl chain length, which results from the interactions between alkyl chains. The previous study has suggested that, the stabilizing interaction between methane dimers mainly arises from the dispersion energy.[64] Therefore, with the increasing length of alkyl chains, a considerable influence of the packing of NDI derivatives arises from an increase in stabilizing dispersion interactions between alkyl chains.

3.3.2 Herringbone stacking. Three BTBT derivatives and two BSBS derivatives adopt the herringbone stacking configuration and display two-dimensional transport behavior presented in Fig. 7. From Table 5, the transfer integrals along π stacking **P1** and **P2** are much larger than for the other pathways. The results of **BTBT-C12** are in accordance with the previous study.[40] As the alkyl chain length increases, the absolute values of transfer integrals along all pathways increase. This is not seen in π–π stacking systems as discussed above. In order to understand the difference, the intermolecular distances and angles between dimers, including the centroid to centroid distances, the perpendicular distance between two BTBT or BSBS core planes, and the displacements along the short and long molecular axis, are listed in Table 5. The short and long molecular axes of BTBT are consistent with those of BSBS defined in Fig. 5. For BTBT derivatives, when the length of alkyl chains increases, the centroid distances and the angle between the rigid π-conjugated skeletons of the dimer along herringbone stacking pathways (**P3–P6**) decrease, contributing to the increased absolute values of transfer integrals.

On the other hand, the absolute values of transfer integrals along the herringbone stacking pathways are from 7 meV to 32 meV for the three systems. And **BTBT-C12** is located at 55° in the mapping of the transfer integral.[40] Obviously, the other two systems also can be found in the range of 0 meV to 50 meV. The decrease of the perpendicular distances between the two BTBT core planes results in the increased absolute values of transfer integrals along **P1** and **P2**. On the other hand, for BSBS derivatives, the decrease of centroid distances and the increase of angles between the rigid π-conjugated skeletons of the dimer along herringbone stacking pathways (**P3–P6**) from **BSBS-C8** to **BSBS-C12** contribute to the increased absolute values of transfer integrals. The obvious increase of the displacements along the short molecular axis, as shown in Table 5, may cause the increased absolute values of transfer integrals along **P1** and **P2**, which can also be found in the two-dimensional contour plot (Fig. 6).

3.4 Charge mobility

Based on the above calculation of parameters, the hopping rates along each pathway are estimated using the quantum charge transfer rate with short time approximation. Then, the kinetic Monte Carlo approach is adopted to simulate the two-dimensional

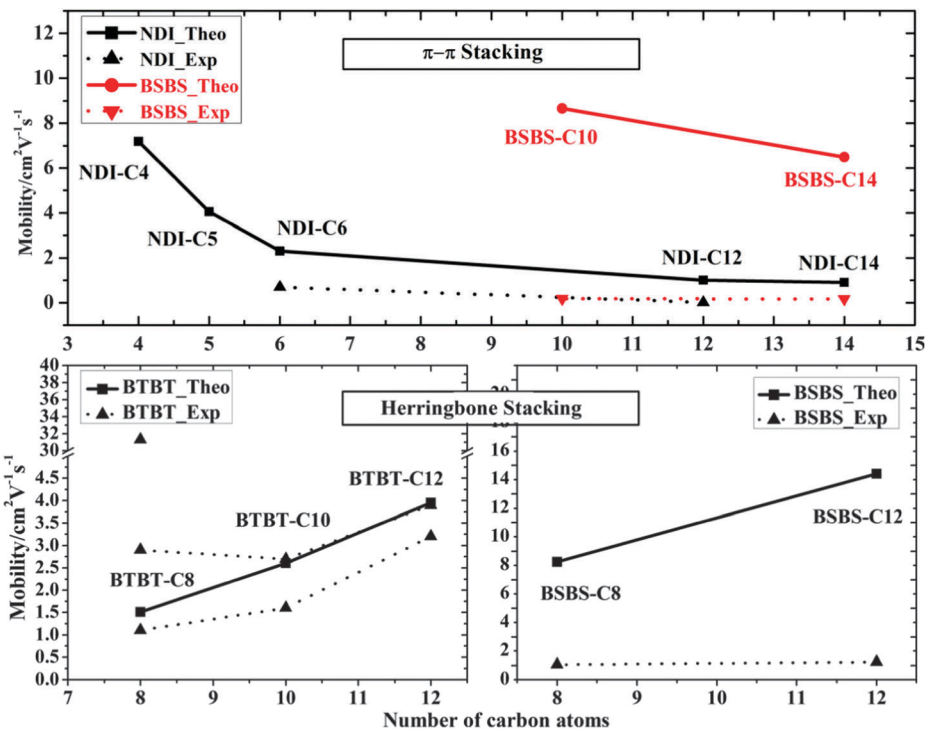

Fig. 8 The charge carrier mobilities from the theoretical calculation and experiment *versus* the number of carbon atoms in alkyl chains.

average electron mobility of NDI derivatives and the two-dimensional average hole mobility of BSBS and BTBT derivatives for the molecular crystals. The calculated results are illustrated in Fig. 8. For comparison, the mobilities from experimental data[31,32,34,36,38] are also illustrated in Fig. 8. The calculated results correlate well in trend with the experiment results for the different kinds of derivatives except **BTBT-C8**, although the absolute mobilities of the systems are different between the calculated results and the experimental results. As presented in Fig. 8, for the π–π stacking systems (NDI derivatives and BSBS derivatives including **BSBS-C10** and **BSBS-C14**), the electron mobilities of NDI derivatives and the hole mobilities of BSBS derivatives decrease as the length of alkyl chains increases. On the other hand, the hole mobilities for the herringbone stacking systems (BTBT derivatives and BSBS derivatives including **BSBS-C8** and **BSBS-C12**) increase as the length of alkyl chains increases.

4. Conclusions

In this work, we have investigated the charge carrier transport properties of two kinds of systems, *i.e.*, π–π stacking systems (NDI derivatives, **BSBS-C10** and **BSBS-C14**) and herringbone stacking systems (BTBT derivatives, **BSBS-C8** and **BSBS-C12**), using the tunneling enabled hopping model coupled with quantum chemistry calculations. We found that the energy levels of frontier molecular orbitals and reorganization energies have negligible changes with respect to the alkyl chain length. Instead, the stabilizing dispersion interactions between alkyl side-chains can change the molecular packing. We find that (i) for the π–π stacking systems (NDI derivatives, **BSBS-C10** and **BSBS-C14**), the displacements along the short molecular axis decrease with alkyl chain length, and the displacements along the long axis adjust correspondingly to form a stable packing arrangement. As a result, the transfer integral in absolute values and the electron mobilities of NDI derivatives and the hole mobilities of BSBS derivatives decrease. (ii) However, for the herringbone stacking systems (BTBT derivatives, **BSBS-C8** and **BSBS-C12**), the centroid distances between the dimers along the herringbone pathways decrease with increasing alkyl chain length. For BTBT systems, in addition to the decreased angles between BTBT cores along the herringbone pathways, the perpendicular distances between the dimers along the π–π stacking pathways also decrease. On the other hand for BSBS derivatives, the increased angles between BSBS cores along the herringbone pathways coupled with the increased displacements along the short molecular axis along the π–π stacking pathways result in an increase of transfer integrals in absolute values. Correspondingly, the hole mobilities of BTBT and BSBS derivatives increase. We believe these findings are helpful for molecular design for synthesizing materials with high carrier mobility.

Acknowledgements

This work was supported by the National Natural Science Foundation of China (Grant no. 21290190, 91333202 and 21303213) and the Ministry of Science and Technology of China (Grant no. 2013CB933503). Computational resources were provided by the Tsinghua Supercomputing Center.

Notes and references

1 A. R. Murphy and J. M. J. Fréchet, *Chem. Rev.*, 2007, **107**, 1066–1096.
2 H. E. Katz, *Chem. Mater.*, 2004, **16**, 4748–4756.
3 J. Kovac, L. Peternai and O. Lengyel, *Thin Solid Films*, 2003, **433**, 22–26.
4 P. K. H. Ho, J.-S. Kim, J. H. Burroughes, H. Becker, S. F. Y. Li, T. M. Brown, F. Cacialli and R. H. Friend, *Nature*, 2000, **404**, 481–484.
5 J. H. Burroughes, D. D. C. Bradley, A. R. Brown, R. N. Marks, K. Mackay, R. H. Friend, P. L. Burns and A. B. Holmes, *Nature*, 1990, **347**, 539–541.
6 K. M. Coakley and M. D. McGehee, *Chem. Mater.*, 2004, **16**, 4533–4542.
7 F. Padinger, R. s. Rittberger and N. s. Sariciftci, *Adv. Funct. Mater.*, 2003, **13**, 85–88.
8 C. J. Brabec, N. S. Sariciftci and J. C. Hummelen, *Adv. Funct. Mater.*, 2001, **11**, 15–26.
9 P. F. Moonen, I. Yakimets and J. Huskens, *Adv. Mater.*, 2012, **24**, 5526–5541.
10 J. Mei, Y. Diao, A. L. Appleton, L. Fang and Z. Bao, *J. Am. Chem. Soc.*, 2013, **135**, 6724–6746.
11 C. Wang, H. Dong, W. Hu, Y. Liu and D. Zhu, *Chem. Rev.*, 2012, **112**, 2208–2267.
12 K. Takimiya, S. Shinamura, I. Osaka and E. Miyazaki, *Adv. Mater.*, 2011, **23**, 4347–4370.
13 P. M. Beaujuge and J. M. J. Fréchet, *J. Am. Chem. Soc.*, 2011, **133**, 20009–20029.
14 J. E. Anthony, *Chem. Rev.*, 2006, **106**, 5028–5048.
15 J. Mei and Z. Bao, *Chem. Mater.*, 2014, **26**, 604–615.
16 T. Lei, J.-Y. Wang and J. Pei, *Chem. Mater.*, 2014, **26**, 594–603.
17 C. Wang, Y. Qin, Y. Sun, Y.-S. Guan, W. Xu and D. Zhu, *ACS Appl. Mater. Interfaces*, 2015, **7**, 15978–15987.
18 S. Chen, B. Sun, W. Hong, H. Aziz, Y. Meng and Y. Li, *J. Mater. Chem. C*, 2014, **2**, 2183–2190.
19 H. Chen, Y. Guo, G. Yu, Y. Zhao, J. Zhang, D. Gao, H. Liu and Y. Liu, *Adv. Mater.*, 2012, **24**, 4618–4622.
20 J. S. Lee, S. K. Son, S. Song, H. Kim, D. R. Lee, K. Kim, M. J. Ko, D. H. Choi, B. Kim and J. H. Cho, *Chem. Mater.*, 2012, **24**, 1316–1323.
21 I. McCulloch, M. Heeney, C. Bailey, K. Genevicius, I. MacDonald, M. Shkunov, D. Sparrowe, S. Tierney, R. Wagner, W. Zhang, M. L. Chabinyc, R. J. Kline, M. D. McGehee and M. F. Toney, *Nat. Mater.*, 2006, **5**, 328–333.
22 B. Fu, J. Baltazar, A. R. Sankar, P.-H. Chu, S. Zhang, D. M. Collard and E. Reichmanis, *Adv. Funct. Mater.*, 2014, **24**, 3734–3744.
23 J.-H. Dou, Y.-Q. Zheng, T. Lei, S.-D. Zhang, Z. Wang, W.-B. Zhang, J.-Y. Wang and J. Pei, *Adv. Funct. Mater.*, 2014, **24**, 6270–6278.

24 T. Lei, J.-H. Dou and J. Pei, *Adv. Mater.*, 2012, **24**, 6457–6461.
25 J. Li, X. Qiao, Y. Xiong, H. Li and D. Zhu, *Chem. Mater.*, 2014, **26**, 5782–5788.
26 F. Zhang, Y. Hu, T. Schuettfort, C. Di, X. Gao, C. R. McNeill, L. Thomsen, S. C. B. Mannsfeld, W. Yuan, H. Sirringhaus and D. Zhu, *J. Am. Chem. Soc.*, 2013, **135**, 2338–2349.
27 H. B. Akkerman, S. C. B. Mannsfeld, A. P. Kaushik, E. Verploegen, L. Burnier, A. P. Zoombelt, J. D. Saathoff, S. Hong, S. Atahan-Evrenk, X. Liu, A. Aspuru-Guzik, M. F. Toney, P. Clancy and Z. Bao, *J. Am. Chem. Soc.*, 2013, **135**, 11006–11014.
28 J. Y. Back, H. Yu, I. Song, I. Kang, H. Ahn, T. J. Shin, S.-K. Kwon, J. H. Oh and Y.-H. Kim, *Chem. Mater.*, 2015, **27**, 1732–1739.
29 J. Liu, Y. Zhang, H. Phan, A. Sharenko, P. Moonsin, B. Walker, V. Promarak and T.-Q. Nguyen, *Adv. Mater.*, 2013, **25**, 3645–3650.
30 S. Inoue, H. Minemawari, J. Tsutsumi, M. Chikamatsu, T. Yamada, S. Horiuchi, M. Tanaka, R. Kumai, M. Yoneya and T. Hasegawa, *Chem. Mater.*, 2015, **27**, 3809–3812.
31 D. Shukla, S. F. Nelson, D. C. Freeman, M. Rajeswaran, W. G. Ahearn, D. M. Meyer and J. T. Carey, *Chem. Mater.*, 2008, **20**, 7486–7491.
32 H. E. Katz, J. Johnson, A. J. Lovinger and W. Li, *J. Am. Chem. Soc.*, 2000, **122**, 7787–7792.
33 W. Jiang, Y. Li and Z. Wang, *Chem. Soc. Rev.*, 2013, **42**, 6113–6127.
34 H. Minemawari, T. Yamada, H. Matsui, J. Tsutsumi, S. Haas, R. Chiba, R. Kumai and T. Hasegawa, *Nature*, 2011, **475**, 364–367.
35 C. Liu, T. Minari, X. Lu, A. Kumatani, K. Takimiya and K. Tsukagoshi, *Adv. Mater.*, 2011, **23**, 523–526.
36 T. Izawa, E. Miyazaki and K. Takimiya, *Adv. Mater.*, 2008, **20**, 3388–3392.
37 H. Ebata, T. Izawa, E. Miyazaki, K. Takimiya, M. Ikeda, H. Kuwabara and T. Yui, *J. Am. Chem. Soc.*, 2007, **129**, 15732–15733.
38 T. Izawa, E. Miyazaki and K. Takimiya, *Chem. Mater.*, 2009, **21**, 903–912.
39 G. Nan and Z. Li, *J. Mater. Chem. C*, 2014, **2**, 1447–1456.
40 H. Kojima and T. Mori, *Bull. Chem. Soc. Jpn.*, 2011, **84**, 1049–1056.
41 G. Nan, X. Yang, L. Wang, Z. Shuai and Y. Zhao, *Phys. Rev. B: Condens. Matter Mater. Phys.*, 2009, **79**, 115203.
42 L. Wang, Q. Li, Z. Shuai, L. Chen and Q. Shi, *Phys. Chem. Chem. Phys.*, 2010, **12**, 3309–3314.
43 H. Geng, Q. Peng, L. Wang, H. Li, Y. Liao, Z. Ma and Z. Shuai, *Adv. Mater.*, 2012, **24**, 3568–3572.
44 X. Yang, Q. Li and Z. Shuai, *Nanotechnology*, 2007, **18**, 424029.
45 E. F. Valeev, V. Coropceanu, D. A. da Silva Filho, S. Salman and J.-L. Brédas, *J. Am. Chem. Soc.*, 2006, **128**, 9882–9886.
46 G. Nan, L. Wang, X. Yang, Z. Shuai and Y. Zhao, *J. Chem. Phys.*, 2009, **130**, 024704.
47 L. Lin, H. Geng, Z. Shuai and Y. Luo, *Org. Electron.*, 2012, **13**, 2763–2772.
48 M. J. Frisch, G. W. Trucks, H. B. Schlegel, G. E. Scuseria, M. A. Robb, J. R. Cheeseman, G. Scalmani, V. Barone, B. Mennucci, G. A. Petersson, H. Nakatsuji, M. Caricato, X. Li, H. P. Hratchian, A. F. Izmaylov, J. Bloino, G. Zheng, J. L. Sonnenberg, M. Hada, M. Ehara, K. Toyota, R. Fukuda, J. Hasegawa, M. Ishida, T. Nakajima, Y. Honda, O. Kitao, H. Nakai, T. Vreven, J. A. Montgomery, Jr., J. E. Peralta, F. Ogliaro, M. Bearpark, J. J. Heyd, E. Brothers, K. N. Kudin, V. N. Staroverov, R. Kobayashi, J. Normand, K. Raghavachari, A. Rendell, J. C. Burant, S. S. Iyengar, J. Tomasi, M. Cossi, N. Rega, J. M. Millam, M. Klene, J. E. Knox, J. B. Cross, V. Bakken, C. Adamo, J. Jaramillo, R. Gomperts, R. E. Stratmann, O. Yazyev, A. J. Austin, R. Cammi, C. Pomelli, J. W. Ochterski, R. L. Martin, K. Morokuma, V. G. Zakrzewski, G. A. Voth, P. Salvador, J. J. Dannenberg, S. Dapprich, A. D. Daniels, O. Farkas, J. B. Foresman, J. V. Ortiz, J. Cioslowski and D. J. Fox, *Gaussian 09*, Gaussian, Inc., Wallingford, CT, 2009.
49 J. R. Reimers, *J. Chem. Phys.*, 2001, **115**, 9103–9109.
50 J. E. Norton and J.-L. Brédas, *J. Am. Chem. Soc.*, 2008, **130**, 12377–12384.
51 J.-L. Brédas, D. Beljonne, V. Coropceanu and J. Cornil, *Chem. Rev.*, 2004, **104**, 4971–5004.
52 B. Jeziorski, R. Moszynski and K. Szalewicz, *Chem. Rev.*, 1994, **7**, 1887–1930.
53 J. M. Turney, A. C. Simmonett, R. M. Parrish, E. G. Hohenstein, F. A. Evangelista, J. T. Fermann, B. J. Mintz, L. A. Burns, J. J. Wilke, M. L. Abrams, N. J. Russ, M. L. Leininger, C. L. Janssen, E. T. Seidl, W. D. Allen, H. F. Schaefer, R. A. King, E. F. Valeev, C. D. Sherrill and T. D. Crawford, *Wiley Interdiscip. Rev.: Comput. Mol. Sci.*, 2012, **2**, 556–565.
54 E. G. Hohenstein and C. D. Sherrill, *J. Chem. Phys.*, 2010, **132**, 184111.
55 E. G. Hohenstein, R. M. Parrish, C. D. Sherrill, J. M. Turney and H. F. S. Iii, *J. Chem. Phys.*, 2011, **135**, 174107.
56 C.-C. Liu, S.-W. Mao and M.-Y. Kuo, *J. Phys. Chem. C*, 2010, **114**, 22316–22321.
57 V. Coropceanu, J. Cornil, D. A. da Silva Filho, Y. Olivier, R. Silbey and J.-L. Brédas, *Chem. Rev.*, 2007, **107**, 926–952.
58 Y. Geng, S.-X. Wu, H.-B. Li, X.-D. Tang, Y. Wu, Z.-M. Su and Y. Liao, *J. Mater. Chem.*, 2011, **21**, 15558.
59 H.-M. Zhao, J. Pfister, V. Settels, M. Renz, M. Kaupp, V. C. Dehm, F. Würthner, R. F. Fink and B. Engels, *J. Am. Chem. Soc.*, 2009, **131**, 15660–15668.
60 R. F. Fink, J. Seibt, V. Engel, M. Renz, M. Kaupp, S. Lochbrunner, H.-M. Zhao, J. Pfister, F. Würthner and B. Engels, *J. Am. Chem. Soc.*, 2008, **130**, 12858–12859.
61 E. Di Donato, R. P. Fornari, S. Di Motta, Y. Li, Z. Wang and F. Negri, *J. Phys. Chem. B*, 2010, **114**, 5327–5334.
62 J. Idé, R. Méreau, L. Ducasse, F. Castet, Y. Olivier, N. Martinelli, J. Cornil and D. Beljonne, *J. Phys. Chem. B*, 2011, **115**, 5593–5603.
63 T. Kakinuma, H. Kojima, M. Ashizawa, H. Matsumoto and T. Mori, *J. Mater. Chem. C*, 2013, **1**, 5395–5401.
64 V. Duarte Alaniz, T. Rocha-Rinza and G. Cuevas, *J. Comput. Chem.*, 2015, **36**, 361–375.